

Phase transition creates the geometry of the continuum from discrete space

Robert S. Farr^{*†} and Thomas M. A. Fink[†]

^{*}*Jacobs Douwe Egberts, Banbury, OX162QU, UK*

[†]*London Institute for Mathematical Sciences, 35a South St, Mayfair, London, UK **

(Dated: Received 27th March 2019. Published 16th August 2019)

Models of discrete space and space-time that exhibit continuum-like behavior at large lengths could have profound implications for physics. They may help tame the infinities arising from quantizing gravity, and remove the need for the machinery of the real numbers; a construct with no direct observational support. However, despite many attempts to build discrete space, researchers have failed to produce even the simplest geometries. Here we investigate graphs as the most elementary discrete models of two-dimensional space. We show that if space is discrete, it must be disordered, by proving that all planar lattice graphs exhibit a taxicab metric similar to square grids. We then give an explicit recipe for growing disordered discrete space by sampling a Boltzmann distribution of graphs at low temperature. Finally, we propose three conditions which any discrete model of Euclid's plane must meet: have a Hausdorff dimension of two, support unique straight lines and obey Pythagoras' theorem. Our model satisfies all three, making it the first discrete model in which continuum-like behavior emerges at large lengths.

PACS numbers: 05.70.Np, 02.50.Ey, 04.20.Gz

I. INTRODUCTION

The small-scale structure of space has puzzled scientists and philosophers throughout history. Zeno of Elea [1] claimed that geometry itself is impossible because there is no consistent form this small-scale structure can take. He argued that a line segment, which can be halved repeatedly, cannot ultimately be composed of pieces of non-zero length, else it would be infinitely long. However, it also cannot be composed of pieces of zero length, for no matter how many are added together, the resulting line will never be longer than zero.

It is a lasting tribute to the optimism of researchers that work on geometry nevertheless carried on. It was not until the 19th century – nearly two and a half millennia later – that Cantor finally resolved the paradox by defining the continuum. He showed that the line must be composed not just of an infinite number of points, but of an uncountably infinite number, so that the second half of Zeno's argument (a proof by induction) fails. This uncountable infinity is described by the mathematical machinery of the real numbers. The continuum is the basis for all descriptions of space and space-time, and therefore all of theoretical physics.

In the 20th century, Weyl [2] further claimed that the continuum is the only possible model of space. He constructed a tiling argument, purporting to show that if space is discrete, Pythagoras' theorem – or, equivalently, the Euclidean metric – is false. Weyl's proof, however, contains an unstated assumption which turns out to be the key to its resolution.

Despite this long belief in the necessity of the con-

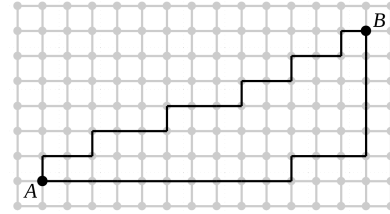


FIG. 1: **The geometry of the square grid graph.** Two nodes *A* and *B* on the square grid graph are separated by 19 edges. There are many possible shortest paths (geodesics) of length 19 edges between the nodes, of which two are shown in black. The resemblance to the possible routes followed by yellow cabs in New York city inspired the term ‘taxicab metric’ for the measure of distance on this graph [16].

tinuum, researchers are actively pursuing discrete [3–5], or at least piece-wise flat [6–10], models of space and space-time, as they offer the possibility to remove non-renormalizable infinities which arise in simple versions of quantum gravity. All these models can be thought of as graphs, where just the graph itself matters, not its embedding into another space. The only natural [11] metric in this case is graph geodesic distance: the distance between two nodes is the smallest number of edges joining them.

In two dimensions, toy models of ‘quantum graphity’ [12] aim to define Hamiltonians over all graphs with a fixed number of nodes, from which an approximation to a smooth manifold might emerge at low temperature. Recent attempts have aimed to produce planar graphs made up of triangles, but, so far [13, 14], the low-temperature phases contain defects, conical singularities and multiply-connected topologies, so are unlike simple, smooth manifolds. A basic feature of such graphs is their Hausdorff dimension, which in this context is the power with which

^{*}Electronic address: robert.farr@JDEcoffee.com; Electronic address: tmafink@gmail.com

the number of nodes in a ball of radius r grows with r . If one deliberately restricts the ensemble of graphs under consideration to triangulations of the plane, a further problem with graph models of two-dimensional space is encountered: Completely random triangulations (i.e. typical graphs chosen at random from this ensemble, and termed ‘Brownian maps’) do not even have Hausdorff dimension two. They are so crumpled that the number of nodes in a disc of radius r scales as r^4 , not r^2 [15].

In light of these difficulties, the prospects for building a consistent discrete model of even the Euclidean plane seem poor. In this Article, we show that it is in fact possible to discretize space. We do three things. First, we prove that any discrete model of two-dimensional space must be disordered, by showing that all planar lattice graphs have a taxicab-like metric [16]. Order is the hidden assumption in Weyl’s proof of the impossibility of discrete space. Second, we describe a local, statistical process, with an associated temperature, which provides an explicit recipe for growing disordered graphs. Third, we propose three tests which any model of Euclidean space must pass. We find that graphs grown by our thermal process, at low temperature, achieve the required properties: they have a Hausdorff dimension of 2, support the existence of unique straight lines, and satisfy Pythagoras’ theorem.

II. LATTICE GRAPHS ARE TAXICAB GRAPHS

The natural way to measure the distance between two nodes on a graph is to count the edges in the shortest path which separates them. A shortest path of this kind is called a geodesic. It is well known that with this measure of distance, the square grid graph has a taxicab geometry [16], where the distance between two nodes is the sum of the magnitude of the differences of their Cartesian coordinates (Figure 1). On this graph there are typically many geodesics between two nodes a distance λ apart, each resembling an irregular staircase. Together these form a geodesic bundle comprising $N_{\text{geo}} \propto \lambda^2$ nodes. More complex lattice graphs show a similar phenomenon (Figure 2a).

In general, any doubly-periodic planar graph must belong to one of the wallpaper groups, familiar from crystallography, and be composed of unit cells containing one or more nodes. We prove that all doubly-periodic planar graphs have the taxicab metric, regardless of the complexity of the unit cell. That is to say, geodesics in all but a finite number of directions form broad, parallelogram bundles (the number of exceptional directions may, however, be large for sufficiently complex unit cells [17]). Such graphs therefore do not satisfy Euclid’s axiom of a unique straight line between two points, nor Pythagoras’ theorem. Our proof is in two parts, which we call geodesic composition and geodesic rearrangement. We sketch the proof here, and give full details in the Methods section.

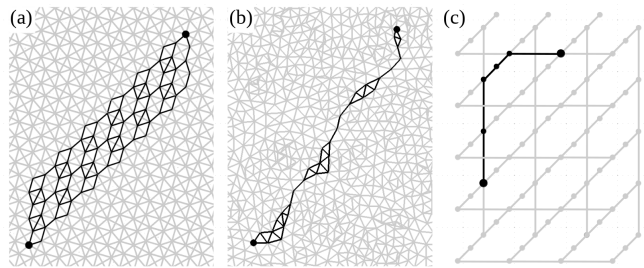


FIG. 2: **Geodesic confinement is not found in planar lattice graphs but is in planar disordered graphs.** (a) In a doubly-periodic triangulation (a modified snub square tiling), two nodes marked as circles are 22 edges apart. We call the set of all geodesics between them (shown in black) the geodesic bundle, containing a number of nodes proportional to the square of the geodesic length. (b) In a random triangulation, the geodesic bundle between two nodes 22 edges apart is confined to a narrow region. We call this phenomenon geodesic confinement. (c) A nonplanar doubly periodic graph (all nodes shown as circles) has neither a taxicab nor Euclidean metric.

Sketch of the proof

If we have a geodesic on a graph between two nodes, it is clear that cutting it in two yields two paths, each of which is a geodesic between its respective end nodes (were that not so, it would be possible to create a shorter path between the original two nodes). Even in classical geometry, however, putting two geodesics (straight lines) end-to-end does not always give a geodesic: they need to be parallel. The situation with graphs is more interesting still.

Equivalent nodes in different unit cells are said to be of the same type. We first construct a geodesic between two nodes of the same type, which are separated by a vector distance of (m, n) unit cells. If we choose the node type so that this is the shortest of all such geodesics (or one of the shortest, if the choice is not unique), then we are able to prove that many copies of this path can be concatenated end-to-end, and the result is still a geodesic between the now widely-separated end points. We call this the geodesic composition property. It is not trivial, since it relies on the assumption of planarity; a nonplanar counterexample is shown in Figure 2c.

Next, we show that a long concatenation of this single type of geodesic can, apart from short tails at the ends, be broken down into many alternating copies of two different geodesics. The proof uses Dedekind’s pigeonhole principle [18], applied to the number of nodes in the unit cell. If m and n are relatively prime, these two geodesics are not parallel. They therefore perform the role of the coordinate directions in the square grid graph and, in the same way, can be re-arranged in any order to produce many irregular staircase-like geodesics, all of the same length. The set of these geodesics forms the broad geodesic bundle, with an area proportional to the square

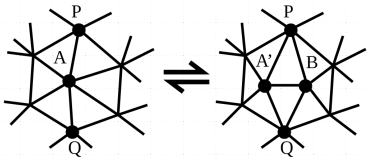


FIG. 3: **Steinitz moves on a portion of a triangulation.** The push move (left to right) consists of choosing a node A and two opposite neighbors P and Q (or nearly opposite, if the degree of A is odd). Node A is divided into nodes A' and B . The pop move (right to left) consists of choosing a node A' , and then one of its neighbors B , which are then merged to a single node A . In contrast to Ref. [20], which keeps track of triangular faces, we avoid tetrahedra and bottlenecks smaller than 4 edges, so faces can be assigned unambiguously, if desired. To ensure no tetrahedra are formed during a pop move, we make an additional check before the merger of A' and B : we require that no neighbor of A' that is not P , Q or B is connected to a neighbor of B that is not P , Q or A' .

of its length – a complete contrast to the narrow lines required by Euclidean geometry.

III. GROWING DISORDERED GRAPHS

In light of the impossibility of generating Euclidean geometry from planar lattice graphs, we turn to disordered graphs which triangulate the 2-sphere. Triangulations here are graphs composed of triangles which, when embedded in the 2-sphere, are planar [19]. We also require that they contain no tetrahedra, so that we only need to keep track of nodes and edges, not faces. As a seed graph, we start from the octahedron (Figure 4), a simple triangulation of the 2-sphere. All triangulations of the 2-sphere are known to be transformable into one another by Steinitz moves [20], illustrated in Figure 3, which are local, and add (‘push’) or remove (‘pop’) nodes while preserving the property of being a triangulation.

We grow the seed graph to a size of N nodes through push moves, and then apply $8N$ alternating push and pop moves to ensure equilibration. This equilibration stage is necessary, since some graph properties (such as mean node eccentricity – see section IV) change slightly, converging (presumably to thermal equilibrium values) after around $4N$ alternating push-pop moves.

Let Z_i be the degree of node i , and $\langle Z \rangle$ the mean degree of all nodes in the triangulation. Because every triangular face has three edges, and every edge belongs to two triangles, Euler’s polyhedron theorem [21] implies that

$$\langle Z \rangle = 6 - 12/N. \quad (1)$$

Since the integrated Gaussian curvature over a smooth, closed surface is 4π [22], we see that $\kappa_i \equiv 6 - Z_i$ is a natural measure of the local, discrete equivalent of Gaussian curvature for the triangulation, up to a constant factor. If we consider a patch of the graph consisting of N_{pat}

nodes, with e exiting edges, and with a simple closed-path perimeter of length $p \geq 3$ edges, then we find the Euler characteristic implies the average discrete curvature over all nodes in the patch is

$$\langle \kappa \rangle_{\text{pat}} = (6 + 2p - e)/N_{\text{pat}}. \quad (2)$$

This can be shown by considering a new triangulation, formed from two copies of the patch, and identifying nodes and edges on the perimeters, then correcting for the exiting edges. Thus a Steinitz push move locally decreases $|\langle \kappa \rangle_{\text{pat}}|$, and a pop move increases it.

To create an ensemble of graphs, we first define an energy E for every graph. We then repeatedly select a random node as a candidate for a push or pop move, and calculate the energy change ΔE that would result. We perform the move with a probability given by the Metropolis algorithm [23] with an associated temperature T . Thus, the move is always accepted if ΔE is negative, and accepted with probability $\exp(-\Delta E/T)$ if ΔE is positive.

Curvature model

The most obvious choice of energy to reduce curvature fluctuations at low temperature is $E_{\text{curv}} = \sum_i \kappa_i^2$, where the sum is over all nodes i . As shown in Figure 4 and also considered in [24], this does indeed drive the local curvature to zero almost everywhere at low temperature, but it does so by creating a branched polymer phase consisting of thin tubes with curvature trapped at their ends and junctions (Figure 4b). The result of this ‘curvature model’ is far from flat. We attribute this to the energy functional failing to sufficiently penalize small curvatures spread over large areas.

Walker model

To address the deficiency of the curvature model, we introduce a second statistical process by putting walkers on the graph. Walker models have previously been used to create both local-cluster structure [25–27], as well as scale-free [28] graphs from local rules [29, 30]; but here we are interested in Euclidean behavior. At each time step, we add κ walkers of type $+1$ to every node with curvature $\kappa > 0$, and $|\kappa|$ walkers of type -1 to every node with $\kappa < 0$. Additionally, 12 walkers of type -1 are added to random nodes to maintain the mean walker number [this requirement can be seen from eq. (1)]. The walkers then diffuse by moving to a random neighboring node. Whenever a $+1$ and a -1 walker occupy the same node, both walkers annihilate. Walker moves alternate with push-pop moves. To define the dynamics, we replace E_{curv} with a new energy E_{walk} for the graph under push-pop moves:

$$E_{\text{walk}} = - \sum_i w_i |w_i|, \quad (3)$$

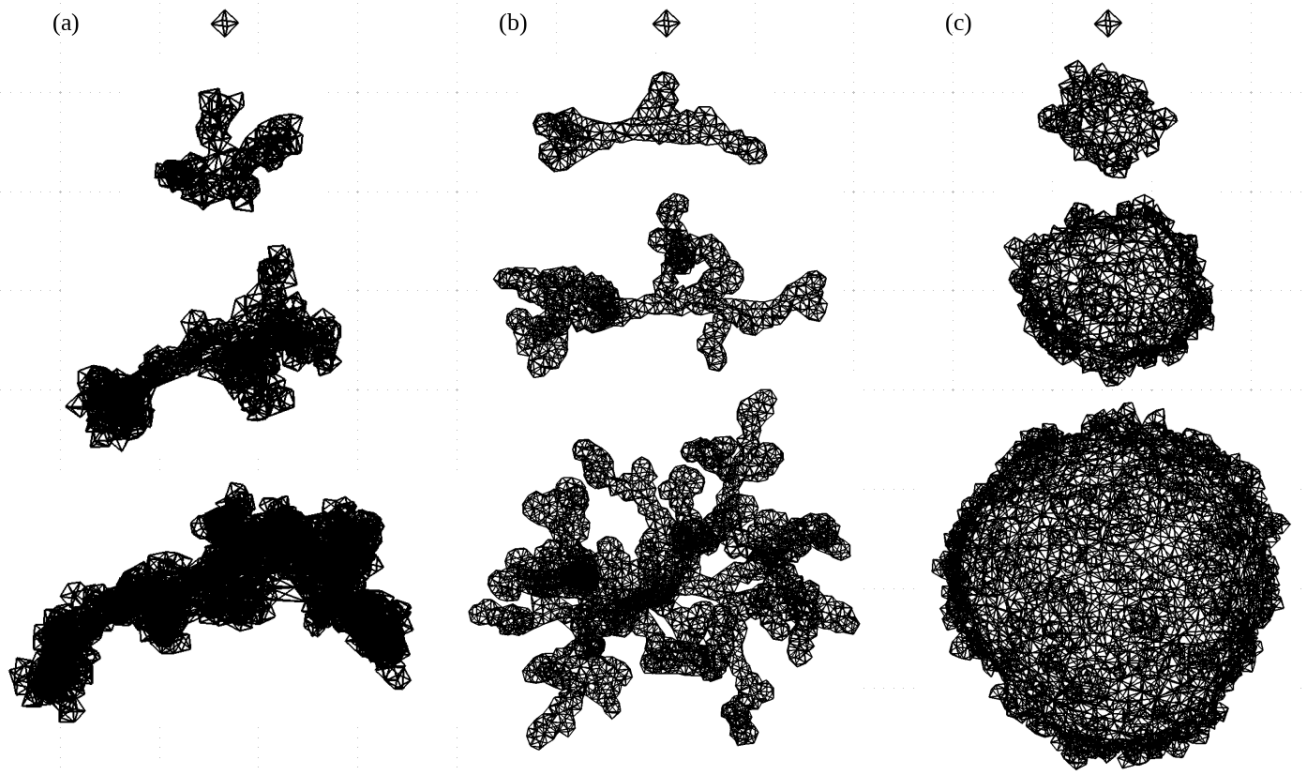


FIG. 4: **Growing graphs at high and low temperatures; the third column shows the main result of this Article: a discrete model of Euclidean space.** A small octahedral triangulation, with $N = 6$ can be grown and equilibrated into larger graphs with $N = 2^8$, 2^{10} and 2^{12} nodes at (a) high temperature, (b) $T = 0.5$ in the curvature model, or (c) low temperature in the walker model. The illustrative embedding into space shown here is irrelevant to our results; we are only interested in the graph.

where w_i is the net number of walkers on node i . At low temperatures, this energy tends to shrink regions of positive curvature and grow regions of negative curvature. We call this new evolution scheme, which biases the graph towards flatness on long length scales, the ‘walker model’.

The walker model generates a triangulation which, at low temperature and long lengths, appears qualitatively to have minimal curvature (Figure 4c). To establish that these graphs satisfy Euclidean geometry at long length scales, we subject them to three tests: a Hausdorff dimension of 2; geodesic confinement; and the Pythagorean theorem.

IV. TESTING OUR GRAPHS

Euclidean geometry is defined through five axioms. These are neither as logically primitive as they first appear, nor do they readily translate into conditions for discrete models of space. We therefore propose three conditions for any discrete model, including ours, purporting to capture Euclid’s geometry at large lengths. The first, Hausdorff dimension, sits outside the original axioms, since they concerned the plane. The second con-

dition is the appearance of straight lines in the large length limit, which we call geodesic confinement. The third is the Euclidean metric itself, commonly known as Pythagoras’ theorem, which is a synthesis of all the axioms.

Hausdorff dimension

If the number of nodes in a ball of radius r scales as $N \propto r^{d_H}$, then d_H is the Hausdorff dimension of the graph. As we noted earlier, planarity is not indicative of dimension: random triangulations of the 2-sphere have $d_H = 4$ as they converge, in the large node limit, to ‘Brownian maps’ [15]. To calculate the dimension of our graphs, we define the half-circumference H of a graph as the average over all nodes of the node eccentricity, where the eccentricity of a node is the greatest geodesic distance between it and any other node in the graph. If nodes are a measure of area, then we would expect a graph which approximates a smooth spherical surface with $d_H = 2$ to satisfy the scaling $H \propto N^{1/2}$. This is not the case for the curvature model (Figure 6a), but is true for the walker model in the low temperature limit for a large number of nodes (Figure 6b). The upwards curvature of the solid

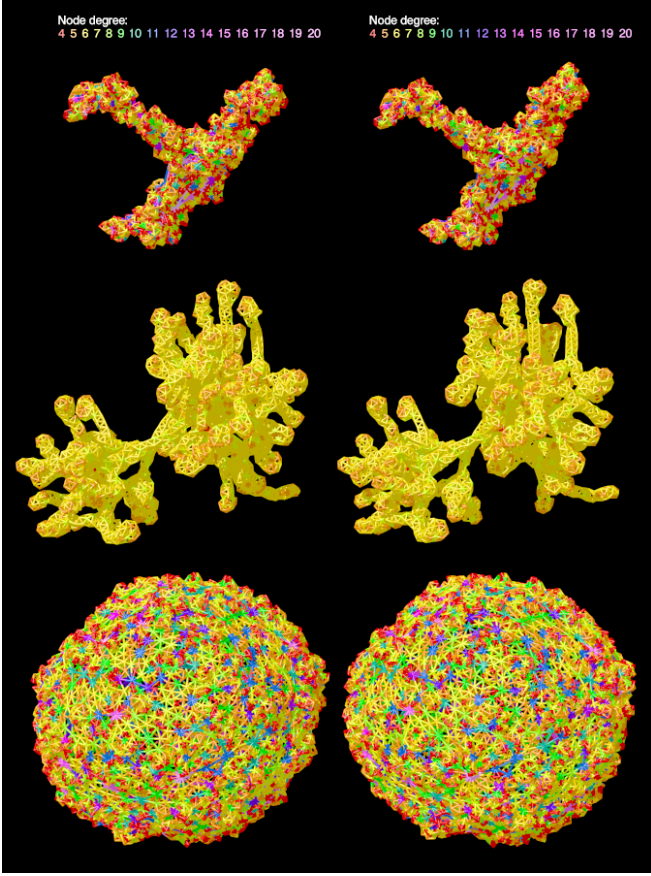


FIG. 5: **Stereograms of graphs with 6144 nodes.** Top two images: high temperature graph. Middle two images: curvature model at $T = 0.5$. Bottom two images: walker model at low temperature. The nodes are coloured according to degree, as shown in the legend at the top of the Figure. To view as stereograms, the Figure should be held approximately 30cm away, while looking through the page until the two images fuse.

gray lines in Figure 6b shows evidence that this $d_H = 2$ phase survives to temperatures above zero.

Geodesic confinement

In a doubly-periodic graph, the total number of nodes N_{geo} in the geodesic bundle between two nodes a distance λ apart scales as $N_{\text{geo}} \propto \lambda^2$. From Figure 6cd, we see that the scaling of N_{geo} with λ also approximates a power law for the low-temperature walker model, but with a different exponent:

$$N_{\text{geo}} \propto \lambda^\gamma \quad \text{with } \gamma \approx 1.1. \quad (4)$$

An exponent $\gamma < 2$ implies qualitatively different behavior to the doubly-periodic lattice case, and in the limit $N \rightarrow \infty$, it is consistent with the narrow geodesics (‘straight lines’) familiar from Euclidean geometry. We call the collapse of the broad, $N_{\text{geo}} \propto \lambda^2$ geodesic bun-

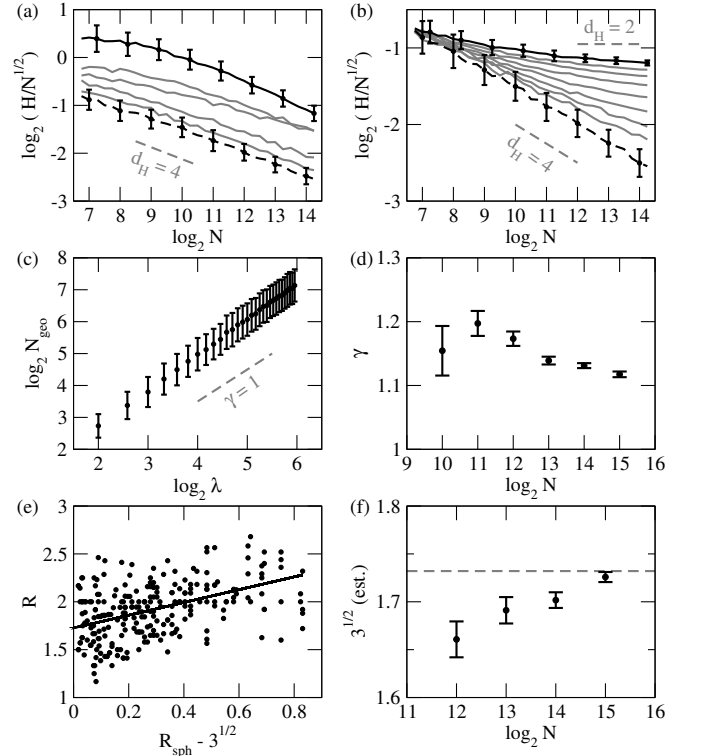


FIG. 6: **Statistical tests for Euclidean behavior of our graphs.** Top row: The mean node eccentricity H and standard deviation for example points, divided by $N^{1/2}$, where N is the number of nodes. (a) The curvature model with $T = 0.5$ (black), $2^0, 2^2, 2^4, 2^6$ (gray) and 10^5 (dashed). (b) The walker model, with $T = 2^{-3}$ (black), $2^2, 2^3, 2^4 \dots 2^8$ (gray) and 10^5 (dashed). Middle row: (c) The number of nodes N_{geo} in geodesic bundles of different lengths λ on a low-temperature walker model graph with $N = 2^{15}$ nodes. (d) Fitted values for γ , where $N_{\text{geo}} \propto \lambda^\gamma$ for graphs of different N . Bottom row: R is the ratio of the perpendicular length to the edge side of an equilateral triangle drawn on a low-temperature walker model with $N = 2^{15}$ nodes. R_{sph} is the exact equivalent on a smooth sphere [eq. (5)]. (e) R plotted against $R_{\text{sph}} - \sqrt{3}$ (we show a random sample of 250 from the full set of 6078 points). The line is a linear regression and we extract the intercept as a graph-theoretic estimate of $\sqrt{3}$. (f) Estimates of $\sqrt{3}$ by this method for graphs of different size N . The dashed gray horizontal line is the exact value.

dles ‘geodesic confinement’ (Figure 2b), by analogy to the flux tubes and color confinement seen in strong-force interactions [31].

Pythagoras’ theorem

Finally, we consider the validity of Pythagoras’ theorem on graphs generated by the walker model. Although this can be proved in general for Euclidean geometry, on graphs we test it empirically by calculating the length of the perpendicular of an equilateral triangle. If Pythag-

Pythagoras' theorem holds, this will be $\sqrt{3}$ times half the side length.

Because we are generating approximations to a spherical surface, rather than a plane, we want to make use of as much of the graph as possible, rather than a small patch on which statistics will be poor. We therefore perform the analogous calculation using spherical, rather than plane trigonometry. If we draw an equilateral spherical triangle on a smooth 2-sphere, with side-length Λ times the half-circumference, the ratio of the length of the perpendicular of the triangle to half its side length will be

$$R_{\text{sph}}(\Lambda) \equiv \frac{2}{\pi\Lambda} \arccos \left[\frac{\cos(\pi\Lambda)}{\cos(\pi\Lambda/2)} \right] = \sqrt{3} + O(\Lambda^2). \quad (5)$$

The same ratio R can be calculated for a graph formed by the low-temperature walker model (Figures 6f, 7), and although the fluctuations are significant, they appear to be unbiased, so that performing linear regression of R against R_{sph} gives an estimate for $\sqrt{3}$ which is only one standard deviation from the traditional value:

$$\sqrt{3}_{\text{est}} = 1.726 \pm 0.005. \quad (6)$$

We believe this is a non-trivial result, unlikely to emerge accidentally, and so we take it as strong evidence that Pythagoras' theorem is satisfied in general for the low-temperature walker model. Since the straightedge and compass operations of drawing circles of any radius, and drawing and measuring (but not extending) lines are simple operations on graphs, many other constructions of classical geometry may readily be tested.

V. METHODS

Our proof that all planar lattice graphs satisfy the taxicab metric is in two parts, which we call geodesic composition and geodesic rearrangement.

Proof of geodesic composition

Consider a doubly-periodic planar graph made up of identical unit cells, each of which comprises ω distinct nodes. Equivalent nodes in different unit cells are said to be of the same type. Let $\mathcal{G}_{pp}(\mathbf{v})$ denote a particular geodesic between two p -type nodes separated by $\mathbf{v} = (m, n)$ unit cells.

We first prove that for any displacement \mathbf{v} , for at least one node type p , the concatenation $\mathcal{G}_{pp}(k\mathbf{v})$ of k copies of $\mathcal{G}_{pp}(\mathbf{v})$ is also a geodesic (Figure 8a–d). Let p be the node type which minimizes $\mathcal{G}_{pp}(\mathbf{v})$. Call this the optimal node assumption. Let p_0p_1 of length $|p_0p_1| = \lambda$ be a geodesic between p_0 and p_1 , which are both of type p , but displaced \mathbf{v} units cells from one another (Figure 8a). Call this the \mathbf{v} -geodesic assumption. Let $p_0p_1p_2$ be two copies of p_0p_1 placed end-to-end.

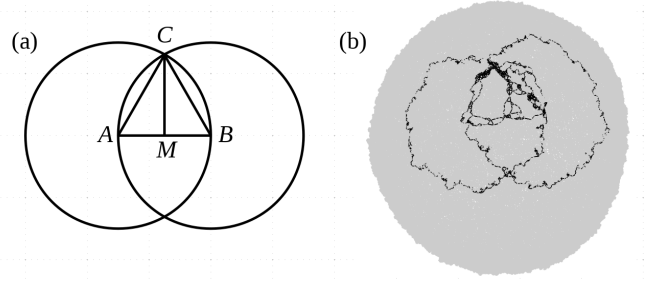


FIG. 7: **Equilateral triangles on the plane and on a graph.** (a) An equilateral triangle drawn on the Euclidean plane with straightedge and compass, where M is half-way between A and B , and $MC/AM = \sqrt{3}$. (b) The same construction using geodesics on a low-temperature 'walker model' graph (which approximates a smooth sphere) with $N = 2^{16}$ nodes and triangle side length of 32.

Now suppose there is a path p_0abp_2 with length $|p_0abp_2| < |p_0p_1p_2| = 2\lambda$ (Figure 8b); because the graph is planar, nodes a and b exist. Then $|ab| < \lambda$ or $|p_0a| + |bp_2| < \lambda$. If the former, then we contradict the optimal node assumption. If the latter, we contradict the \mathbf{v} -geodesic assumption. Therefore $p_0p_1p_2$ is a geodesic between p_0 and p_2 . That is to say, $\mathcal{G}_{pp}(2\mathbf{v})$, which is the concatenation of 2 copies of $\mathcal{G}_{pp}(\mathbf{v})$, is a geodesic. Call this the $2\mathbf{v}$ -geodesic property.

We now show that the $(k-1)\mathbf{v}$ -geodesic property implies the $k\mathbf{v}$ -geodesic property (Figure 8c for $k=3$). Suppose there is a path p_0abp_k with length $|p_0abp_k| < |p_0p_1 \dots p_k| = k\lambda$. Then $|ab| < \lambda$ or $|p_0a| + |bp_k| < (k-1)\lambda$ (Figure 8d for $k=3$). If the former, then we contradict the optimal node assumption. If the latter, then we contradict the $(k-1)\mathbf{v}$ -geodesic property. Therefore $p_0p_1 \dots p_k$ is a geodesic between p_0 and p_k . This completes the first part of the proof.

Proof of geodesic rearrangement

We next prove that for most displacements \mathbf{v} , for at least one node type p , the geodesic $\mathcal{G}_{pp}(k\mathbf{v})$ consists of three parts: a tail at each end, which joins the nodes p_0 and p_k to copies of some other type of node q , and between the tails, $k-1$ alternating copies of $\mathcal{G}_{qq}(\mathbf{u})$ and $\mathcal{G}_{qq}(\mathbf{u}')$ for some displacement vectors \mathbf{u} and \mathbf{u}' (Figure 8ef). We now only consider displacement vectors $\mathbf{v} = (m, n)$ such that m and n are relatively prime (which occurs [32] for random m and n with probability $6/\pi^2 \simeq 0.61$) and large enough so that $\lambda > 2\omega$, where ω is the number of distinct nodes in the unit cell. By Dedekind's pigeonhole principle [18], since $\lambda/\omega > 2$, $\mathcal{G}_{pp}(\mathbf{v})$ must pass through at least two nodes of some other type q different from type p (Figure 8e). Therefore we can define a sub-geodesic $\mathcal{G}_{qq}(\mathbf{u})$ within $\mathcal{G}_{pp}(\mathbf{v})$, and a second geodesic $\mathcal{G}_{qq}(\mathbf{u}')$ between the node q in adjacent copies of $\mathcal{G}_{pp}(\mathbf{v})$ (Figure 8f).

Because m and n are relatively prime, \mathbf{u} and \mathbf{u}' cannot

pled objects, confined in a small region of space. However, the irregular, jagged curvature of the crumpled phase is entirely extrinsic: a function of its embedding in three-dimensional space. The intrinsic, ordered, taxicab geometry of the membrane itself is unchanged through the crumpling transition.

In contrast, the phase transition we find at low temperature in the walker model changes the *intrinsic* metric of the graph from a crumpled, non-Euclidean ‘Brownian map’ [15] into smooth, Euclidean space. It is unclear, at present, whether the phase transition occurs at finite or infinite temperature. A renormalization group analysis of the model may shed light on this question.

Walker model

The phase transition which creates continuum geometry is driven by a statistical walker process. The motivation for this comes from the naïve curvature model, which minimizes the sum of the squares of the local discrete curvature κ , but disappointingly gives rise to a ‘Medusa’ phase (Figure 4b). This pathological behavior is consistent with previous investigations of triangulations, which lead to branched polymer phases and other exotic geometries rather than smooth, homogenous space [24, 35]. The pathologies are due to concentrations of discrete curvature in confined regions; in other words, large, local curvature fluctuations. Our walker process – which solves a discrete version of Poisson’s equation, with the charge being the curvature κ – is sensitive to small curvatures on large length scales, and so, through the energy functional E_{walk} , ultimately acts to spread these fluctuations over the whole graph.

A background for simulations

A practical application of our Euclidean graphs is as a background for simulations. Lattices, such as the square grid, are intrinsically anisotropic, so special care is often needed when designing simulations to run on them. The rotational symmetry of our graphs therefore make them suitable spaces on which to perform algorithms such as lattice gas cellular automata [36].

Higher dimensions

We have built a discrete, graph model that behaves like two-dimensional Euclidean space at large lengths. Can the same be done for higher dimensions? While more computationally intensive, our walker model should generalize naturally to dimensions greater than two. In three dimensions, the key step is extending the Steinitz moves in Figure 3 to add and subtract tetrahedra, rather than

triangles, as nodes divide and fuse. Whether the resulting graph will be Euclidean is, however, unknown. Our tests for geodesic confinement and the applicability of Pythagoras’ theorem are benchmarks for this and any other discrete models attempting to capture Euclidean geometry at large lengths.

We conjecture that the absence of geodesic confinement carries over to higher dimensional lattices, as it clearly does for the three-dimensional regular cubic grid. Unfortunately, the proof does not readily follow from our theorem in two dimensions, which relies on planarity, since all three-dimensional lattices are non-planar. Figure 2c gives an indication of the subtlety. It shows a non-planar, two-dimensional lattice not satisfying geodesic composition, a key step in our proof (see Methods).

Closely related results have been proved for more general cases. It is known that for asymptotically large radii, balls around a node in a lattice graph of any dimension can never be ellipsoids, but are rational polytopes [17]. Isotropic behavior of geodesics is therefore impossible, and if these polytopes were exact, rather than having finite length whiskers in certain directions (the eventuality of Figure 2c) broad geodesic bundles would follow from the partial incidence of the faces of polytopes of radius r around two points separated by $2r$.

The Minkowski metric

We have shown how to grow graphs with a Euclidean metric, that is, that satisfy Pythagoras’ theorem, $d^2 = x^2 + y^2$, where d is distance and x and y orthogonal directions. What about other metrics? The most important is the Minkowski metric of special relativity, the two-dimensional analog of which is $d^2 = t^2 - x^2$, where t is a time direction. How to represent this as a graph is an open question, because nodes must be intricately connected at large coordinate displacements. Taking an approach similar to causal set theory [3, 4], but with neighbors separated by unit proper time, would suggest that the degree of each node diverges with the logarithm of the volume of space-time (or worse, as a power, for higher dimensions). Furthermore, unlike Euclidean space, where the square grid graph at least models a 4-fold rotational symmetry, it is not possible to construct a lattice graph which is symmetric under even a discrete version of the Lorentz transformation. Thus, it remains to be seen whether some variant of the walker process can be defined to probe and engender the fabric of space-time.

Acknowledgments

The authors thank Prof. Yang-Hui He and Dr Ilia Teimouri for useful discussions.

-
- [1] A. Hagar A, *Discrete or continuous? The quest for fundamental length in modern physics*, (Cambridge University Press, Cambridge, England, 2014).
- [2] H. Weyl, *Philosophy of mathematics and the natural sciences* (Princeton University Press, Princeton, US, 1949).
- [3] L. Bombelli, J. Lee, D. Meyer and R.D. Sorkin, *Spacetime as a causal set*, Phys. Rev. Lett. **59**, 521 (1987).
- [4] D.M.T. Benincasa and F. Dowker, *Scalar curvature of a causal set*, Phys. Rev. Lett. **104**, 181301 (2010).
- [5] A. Hama, F. Markopoulou, S. Lloyd, F. Caravelli, S. Severini and K. Markström, *Quantum Bose-Hubbard model with an evolving graph as a toy model for emergent spacetime*, Phys. Rev. D, **81**, 104032 (2010).
- [6] T. Regge, *General relativity without coordinates*, Nuovo Cimento **19**, 558 (1961).
- [7] T. Regge and R.M. Williams, *Discrete structures in gravity*, J. Math. Phys. **41**, 3964 (2000).
- [8] J. Ambjørn, J. Jurkiewicz and R. Loll, *Spectral dimension of the universe*, Phys. Rev. Lett. **95**, 171301 (2005).
- [9] J. Ambjørn, J. Jurkiewicz and R. Loll, *Emergence of a 4D world from causal quantum gravity*, Phys. Rev. Lett. **93**, 131301 (2004).
- [10] P. Horava, *Spectral dimension of the universe in quantum gravity at a Lifshitz point*, Phys. Rev. Lett. **102**, 161301 (2009).
- [11] F. Leymarie and M.D. Levine, *Fast raster scan distance propagation on the discrete rectangular lattice*, CVGIP: Image Understanding **55**(1), 84 (1992).
- [12] T. Konopka, F. Markopoulou and S. Severini, *Quantum gravity: a model of emergent locality*, Phys. Rev. D **77**(10), 104029 (2008).
- [13] F. Conrady, *Space as a low-temperature regime of graphs*, J. Stat. Phys. **142**, 898 (2011).
- [14] S. Chen and S. Plotkin, *Statistical mechanics of graph models and their implications for emergent spacetime manifolds*, Phys. Rev. D **87**, 084011 (2013).
- [15] J.F. le Gall, *Random geometry on the sphere*, Proc. Int. Congr. Math. Seoul, **1**, 421 (2014).
- [16] E.F. Krause, *Taxicab geometry, an adventure in non-Euclidean geometry* (Addison-Wesley, Boston, US, 1975).
- [17] T. Fritz, *Velocity polytopes of periodic graphs and a no-go theorem for digital physics*, Discrete Mathematics **313**(12), 1289 (2011).
- [18] P. Erdős and R. Rado, *A partition calculus in set theory*, Bull. Am. Math. Soc. **62**, 427 (1956).
- [19] F.H. Lutz, *Enumeration and Random Realization of Triangulated Surfaces*. In: A.I. Bobenko, J.M. Sullivan, P. Schröder and G.M. Ziegler (eds.), *Discrete Differential Geometry*, (Oberwolfach Seminars, Vol. 38, Birkhäuser, Basel, 2008).
- [20] E. Steinitz and H. Rademacher, *Vorlesungen über die Theorie der Polyeder* (Springer, 1934).
- [21] L. Euler, *Elementa doctrinae solidorum*, Novi Comm. Acad. Sci. Imp. Petropol. **4**, 109 (1752-3).
- [22] O. Bonnet, *Mémoire sur la théorie générale des surfaces*, J. École Polytechnique, **19**, 1 (1848).
- [23] N. Metropolis, A.W. Rosenbluth, M.N. Rosenbluth, A.H. Teller and E. Teller, *Equations of state calculations by fast computing machines*, J. Chem. Phys. **21**, 1087 (1953).
- [24] T. Aste and D. Sherrington, *Glass transition in self-organizing cellular patterns*, J. Phys. A: Mathematical and General **32**, 7049 (1999).
- [25] N. Ikeda, *Network formation determined by the diffusion process of random walkers*, J. Phys. A: Mathematical and Theoretical **41** 235005 (2008).
- [26] A. Vázquez, *Growing network with local rules: Preferential attachment, clustering hierarchy, and degree correlations*, Phys. Rev. E **67**, 056104 (2003).
- [27] R. Toivonen, J-P. Onnela, J. Saramäki, J. Hyvönen and K. Kaski, *A model for social networks*, Physica A **371**(2), 851 (2006).
- [28] P.L. Krapivsky, S. Redner and F. Leyvraz, *Connectivity of growing random networks*, Phys. Rev. Lett. **85**, 4629 (2000).
- [29] J. Saramäki and K. Kaski, *Scale-free networks generated by random walkers*, Physica A **341**, 80 (2004).
- [30] F. Caravelli, A. Hama and M. Di Ventura, *Scale-free networks as an epiphenomenon of memory*, EPL **109**, 28006 (2015).
- [31] K.G. Wilson, *Confinement of quarks*, Phys. Rev. D **10**, 2445 (1974).
- [32] G.H. Hardy and E.M. Wright, *An introduction to the theory of numbers* (Oxford University Press, Oxford, England, 2008).
- [33] W.K. Burton, N. Cabrera and F.C. Frank, *The growth of crystals and the equilibrium structure of their surfaces*, Proc. R. Soc. Lond. A **243**, 299 (1951).
- [34] M.J. Bowick and A. Travesset, *The statistical mechanics of membranes*, Phys. Reports **344**, 255 (2001).
- [35] R. Gurau and J. Ryan, *Melons are branched polymers*, Annales Henri Poincaré **15**, 2085 (2014).
- [36] U. Frisch, B. Hasslacher and Y. Pomeau, *Lattice-gas automata for the Navier-Stokes equation*, Phys. Rev. Lett. **56**, 1505 (1986).